


Article

Innovative In/H-SSZ-39 Catalysts: An Exploration in NO_x Reduction via CH₄-SCR

Jiuhu Zhao ^{1,2,3,†}, Jingjing Jiang ^{1,†}, Meng Wang ^{1,2,†}, Jianxiong Chen ^{1,2}, Jin Li ⁴, Xianbin Wang ⁴ and Rongshu Zhu ^{1,2,*} ¹ State Key Laboratory of Urban Water Resource and Environment, School of Economics and Management, Harbin Institute of Technology Shenzhen, Shenzhen 518055, China² Shenzhen Key Laboratory of Organic Pollution Prevention and Control, School of Civil and Environmental Engineering, Harbin Institute of Technology Shenzhen, Shenzhen 518055, China³ Shenzhen Government Investment Project Evaluation Center, Shenzhen 518036, China⁴ China Catalyst Holding Co., Ltd., Dalian 116308, China

* Correspondence: rszhu@hit.edu.cn

† These authors contributed equally to this work.

Abstract: Nitrogen oxides (NO_x), pivotal atmospheric pollutants, significantly threaten the environment and human health. The CH₄-SCR process, leveraging the abundance and accessibility have methane, emerges as a promising avenue for NO_x abatement. Previous studies have demonstrated that zeolite support with twelve-membered ring (12-MR) and five-membered ring (5-MR) structures are susceptible to framework collapse in the presence of H₂O, leading to catalyst deactivation. Consequently, there is a necessity to explore novel zeolites with enhanced hydrothermal stability for application in CH₄-SCR processes. This research introduced for the first time an investigation into a novel In/H-SSZ-39 catalyst, which was synthesized via ion exchange and meticulously optimized for preparation conditions, including calcination temperature and In ions concentration, and reaction conditions, including CH₄/NO ratio, O₂ concentration, H₂O content, and Gas Hourly Space Velocity (GHSV). Furthermore, long-term operation tests and stability tests were conducted on the In/H-SSZ-39 catalyst. In addition, a series of characterizations were conducted to delve into the reasons behind how preparation conditions influence catalytic activity, as well as to investigate the changes in physicochemical properties during the reaction process.

Keywords: CH₄-SCR; In/H-SSZ-39; catalytic performance; preparation condition; reaction condition; physicochemical properties



Citation: Zhao, J.; Jiang, J.; Wang, M.; Chen, J.; Li, J.; Wang, X.; Zhu, R. Innovative In/H-SSZ-39 Catalysts: An Exploration in NO_x Reduction via CH₄-SCR. *Catalysts* **2024**, *14*, 582. <https://doi.org/10.3390/catal14090582>

Academic Editors: Giuseppe Bonura, Jong-Ki Jeon and Andrea Goti

Received: 23 June 2024

Revised: 16 August 2024

Accepted: 30 August 2024

Published: 1 September 2024



Copyright: © 2024 by the authors. Licensee MDPI, Basel, Switzerland. This article is an open access article distributed under the terms and conditions of the Creative Commons Attribution (CC BY) license (<https://creativecommons.org/licenses/by/4.0/>).

1. Introduction

Nitrogen oxides (NO_x) are a major component of atmospheric pollution, primarily emanating from energy use, industrial production, and transportation-activities [1]. NO_x contributes to a range of ecological and environmental issues, including acid rain, photochemical smog, and the exacerbation of the greenhouse effect. Moreover, it poses a significant threat to human health by triggering respiratory diseases. Therefore, the removal of NO_x from the atmosphere is imperative for preserving a clean environment and safeguarding public health [2,3].

Among the various DeNO_x technologies, selective catalytic reduction (SCR) has garnered significant research interest. This is due to its ability to facilitate the chemical reaction between NO_x in exhaust gases and a reducing agent, in the presence of a catalyst, converting NO_x into environmentally harmless N₂ [4]. In particular, methane-selective catalytic reduction (CH₄-SCR) technology utilizes methane (CH₄) as a reductant. This method has several advantages, including the abundant availability, cost-effectiveness, and ease of sourcing methane, which suggests a promising future for CH₄-SCR technology in widespread applications [5].

Catalysts constitute a key element of CH₄-SCR DeNO_x technology. In recent years, extensive research has been conducted on zeolite-supported catalysts featuring twelve-membered or five-membered rings, which are pivotal in various catalytic processes [6]. However, it has been discovered that these catalysts are prone to framework collapse under aqueous conditions, which significantly compromises their structural integrity and catalytic performance [7]. Identifying a novel zeolite support is pivotal for addressing the issue of catalyst deactivation induced by steam poisoning.

Kwak et al. [8] have reported that the copper-based zeolite Cu-SSZ-13, characterized by a CHA-type framework, demonstrates commendable catalytic efficacy in NH₃-SCR fields. However, its performance is compromised following thermal treatments exceeding 850 °C, which necessitates a reduction in its high-temperature hydrothermal stability. Consequently, there is an imperative to not only augment the thermal resilience of Cu-SSZ-13 but also to innovate and introduce novel catalytic supports with enhanced robustness. In this vein, a variety of newly synthesized copper-impregnated zeolites with small pores (non-CHA type) have been subjected to NH₃-SCR performance assessments. Studies have documented that Cu-LTA [9,10], Cu-KFI [11], and Cu-AEI [12,13] exhibit promising catalytic profiles. Notably, the Cu-SSZ-39 zeolite, which incorporates an AEI-type structure and features cage-like channels with expanded dimensions (3.8 × 3.8 Å), has been highlighted for its exceptional hydrothermal stability and commendable NH₃-SCR catalytic activity [14,15]. Fickel et al. [16] have observed that Cu-SSZ-39 outperforms mesoporous and microporous zeolites in terms of both catalytic activity and hydrothermal stability during NH₃-SCR reactions. Du [17] has conducted an in-depth investigation into the eight-membered ring channel architecture of Cu-SSZ-39 zeolite, revealing its superior activity under hydrothermal conditions when juxtaposed with Cu-SSZ-13. Remarkably, it sustains its denitration proficiency even after enduring hydrothermal aging at 850 °C for a duration of 16 h. The underlying rationale for this enhanced performance is attributed to the more convoluted channel configuration of SSZ-39 zeolite in contrast to its SSZ-13 counterpart, which effectively mitigates the leaching of aluminum elements and the aggregation of copper species induced by hydrothermal aging. Despite the advancements in CH₄-SCR technology, there is a notable scarcity of research pertaining to catalysts loaded with SSZ-39 zeolites. This observation underscores the potential for further investigation and development in this area.

Based on this, the objective of this research is to synthesize an innovative In/H-SSZ-39 catalyst and to optimize the conditions for its preparation, specifically focusing on the In ions concentration and the calcination temperature. The optimization process will be guided by the evaluation of the catalytic performance in CH₄-SCR denitration processes. Subsequently, the catalytic activity of the optimized In/H-SSZ-39 catalyst will be assessed under a variety of reaction conditions. These conditions include the concentration of O₂, the CH₄ to NO ratio, the Gas Hourly Space Velocity (GHSV), and the concentration of H₂O. Furthermore, a meticulous analysis was conducted to delve into the interplay between the catalytic activity and the various preparation conditions.

2. Results and Discussion

2.1. Effect of Preparation Conditions

2.1.1. Si/Al Ratio

The Si/Al ratio is a determinant factor in modulating the acidity of catalysts, which significantly influences catalytic performance [18]. Zeolites with Si/Al ratios of 16 and 4.9 were utilized as supports to fabricate In/H-SSZ-39 catalysts. The synthesis was standardized with an ion-exchange solution concentration of 0.066 M and a calcination temperature of 500 °C. The catalytic performance of the resultant catalysts was assessed for CH₄-SCR DeNO_x under standardized reaction conditions: 400 ppm NO, 600 ppm CH₄, 10% O₂, 6% H₂O, and a GHSV of 21,000 h⁻¹.

Analysis of Figure 1 reveals that the In/H-SSZ-39 catalyst with a Si/Al ratio of 16 exhibited a NO_x removal efficiency of 42.1%, contrasting with the 15.0% DeNO_x efficiency of

the catalyst with a Si/Al ratio of 4.9. This disparity underscores the substantial impact of the Si/Al ratio on catalytic activity. A catalyst with a low Si/Al ratio was characterized by reduced acidity, which correlated with a diminished number of active sites, thereby adversely affecting the CH₄-SCR reaction [7]. The comparisons of catalytic performance with other In-zeolites catalysts are listed in Table 1 [19–21]. As evident from the data presented in Table 1, it was observed that the catalytic activity of Beta, SSZ-13, and SSZ-39 zeolite-supported catalysts exhibited varying performance under different reaction conditions. Specifically, the catalytic activity of In/H-SSZ-39 under high space velocity and low oxygen conditions warranted further investigation when compared to In/H-SSZ-13 catalysts.

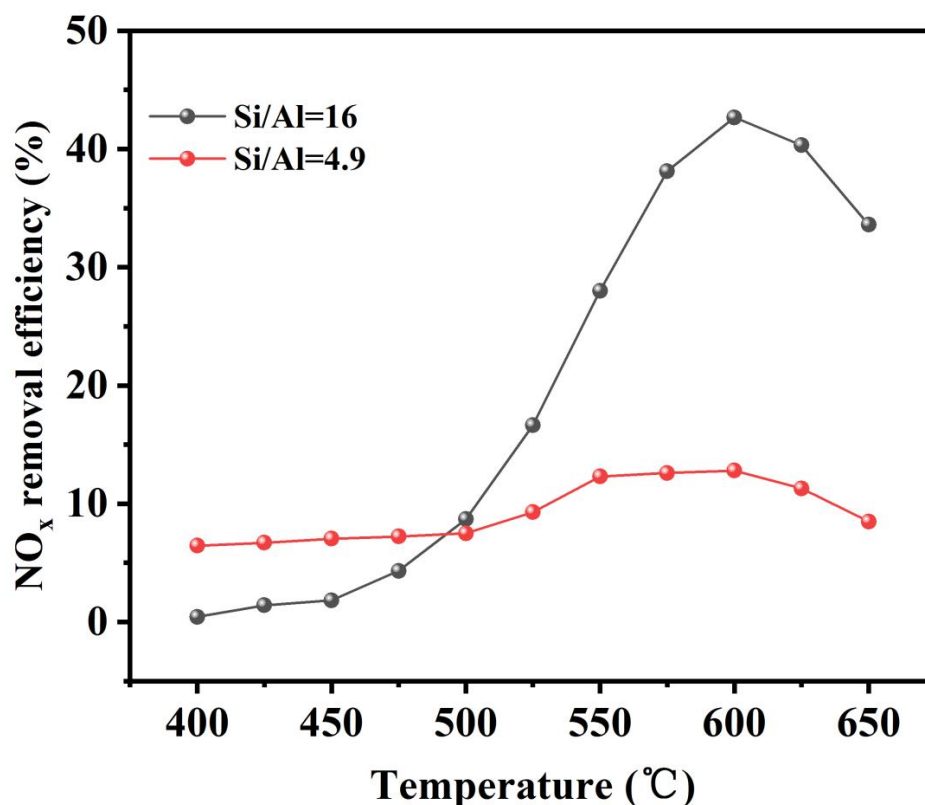


Figure 1. Catalytic performance of the In/H-SSZ-39 catalysts with various Si/Al ratios.

Table 1. Comparison of catalytic performance with other In-zeolites catalysts.

| Catalyst | Reaction Conditions | NO _x Removal Efficiency (%) | Reaction Temperature (°C) | Reference |
|-------------|--|--|---------------------------|-----------|
| Co-Beta | 2180 ppm NO, 2050 ppm CH ₄ , 2% O ₂ , 78 ppm SO ₂ , and a GHSV of 7500 h ⁻¹ | 32% | 600 | [19] |
| In/H-Beta | 400 ppm NO, 400 ppm CH ₄ , 10% O ₂ , 100 ppm SO ₂ , 5% H ₂ O, and a GHSV of 23,600 h ⁻¹ | 31% | 600 | [6] |
| In/H-Beta-P | 400 ppm NO, 400 ppm CH ₄ , 10% O ₂ , 100 ppm SO ₂ , 5% H ₂ O, and a GHSV of 23,600 h ⁻¹ | 40% | 650 | [20] |
| In/H-SSZ-13 | 2500 ppm NO, 4000 ppm CH ₄ , 4% O ₂ , 6% H ₂ O, and a GHSV of 75,000 h ⁻¹ | 38% | 500 | [21] |
| In/H-SSZ-39 | 400 ppm NO, 600 ppm CH ₄ , 10% O ₂ , 6% H ₂ O, and a GHSV of 21,000 h ⁻¹ | 42.1% | 625 | Our work |

Upon conducting ICP analysis (Table 2), it was observed that the In/H-SSZ-39 catalysts exhibited relatively close In loading capacities when possessing Si/Al ratios of 4.9 and 16, respectively. Moreover, the Si/Al ratio could affect the surface acidity of catalysts [18]. NH₃-TPD characterization was carried out to investigate the relationship between the silicon–aluminum ratio and acid content. The NH₃-TPD profiles of In/H-SSZ-39 catalysts with silicon–aluminum ratios of 4.9 and 16 are presented in Figure 2. These profiles have been deconvoluted into three distinct peaks: Peak I, attributed to weak acid sites; Peak II, assigned to medium acid sites; and Peak III, ascribed to strong acid sites [18,22]. The results of the NH₃-TPD curve fitting are summarized in Table 3. Notably, the total acid quantity of In/H-SSZ-39 (Si/Al = 16) exhibited a higher acid quantity compared to In/H-SSZ-39 (Si/Al = 4.9), which is in good agreement with the observed CH₄-SCR performance trends (Figure 1), thereby reinforcing the pivotal role of acid sites in facilitating DeNO_x catalysis.

Table 2. Compositional analysis of the In/H-SSZ-39 samples.

| Catalysts | Content of In (wt.%) | Content of Al (wt.%) | Content of Si (wt.%) | Si/Al |
|---------------------------|----------------------|----------------------|----------------------|-------|
| In/H-SSZ-39 (Si/Al = 4.9) | 5.68 | 3.98 | 19.50 | 4.9 |
| In/H-SSZ-39 (Si/Al = 16) | 5.5 | 2.45 | 40.33 | 16 |
| Used In/H-SSZ-39 | 5.1 | 2.47 | 41.31 | 16 |

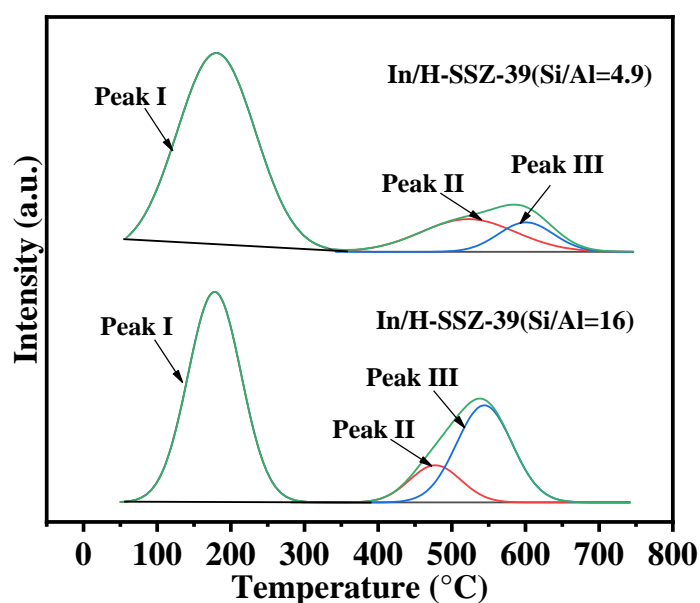


Figure 2. NH₃-TPD plots of the In/H-SSZ-39 (Si/Al = 4.9) and In/H-SSZ-39 (Si/Al = 16) catalysts.

Table 3. The amount of surface acid sites over obvious In/H-SSZ-39 catalysts.

| Sample | Peak I | | Peak II | | Peak III | | Q _{total} (mmol g ⁻¹) |
|---------------------------|--------|---------------------------|---------|---------------------------|----------|---------------------------|--|
| | T (°C) | Q (mmol g ⁻¹) | T (°C) | Q (mmol g ⁻¹) | T (°C) | Q (mmol g ⁻¹) | |
| In/H-SSZ-39 (Si/Al = 16) | 178 | 1.098 | 477 | 0.186 | 546 | 0.529 | 1.813 |
| In/H-SSZ-39 (Si/Al = 4.9) | 168 | 1.045 | 489 | 0.209 | 560 | 0.110 | 1.365 |
| Used In/H-SSZ-39 | 175 | 1.022 | 466 | 0.186 | 579 | 0.434 | 1.642 |

2.1.2. Effect of Calcination Temperature

The In/H-SSZ-39 catalysts were synthesized and their catalytic performance was evaluated under various calcination temperatures (450 °C, 500 °C, 550 °C, and 600 °C) with the ion-exchange solution concentration maintained at 0.066 M. The experimental conditions were standardized as follows: 400 ppm NO, 600 ppm CH₄, 10% O₂, 6% H₂O, and a GHSV of 21,000 h⁻¹. The results are depicted in Figure 3a–c.

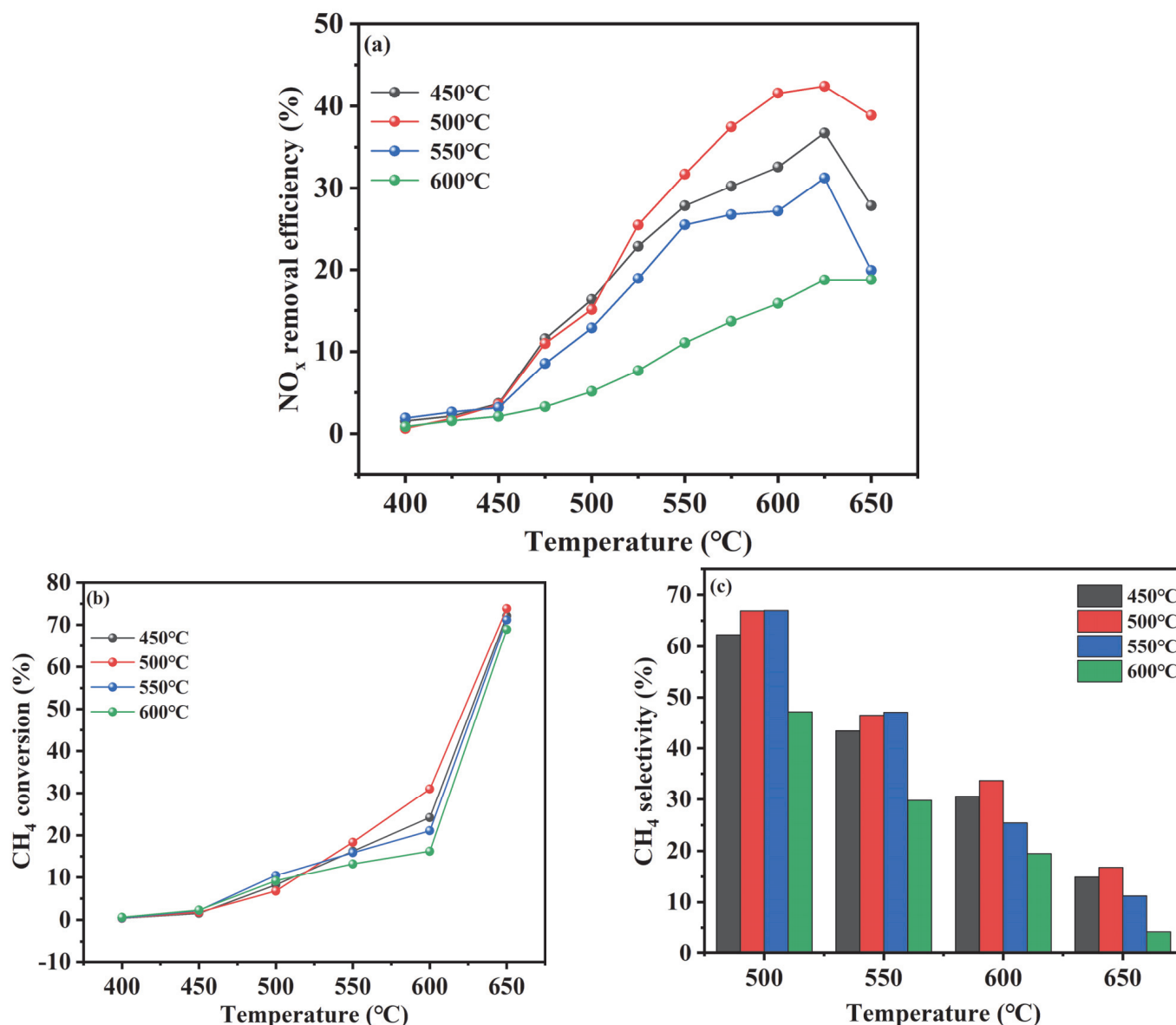


Figure 3. Catalytic performance of the In/H-SSZ-39 catalysts with various calcination temperatures. (a) NO_x removal efficiency, (b) CH₄ conversion, and (c) CH₄ selectivity.

Figure 3a illustrates the catalytic performance of the In/H-SSZ-39 catalysts prepared at different calcination temperatures. It was observed that the catalytic activity initially increased with temperature and then declined. The In/H-SSZ-39 catalyst calcined at 500 °C demonstrated the highest DeNO_x efficiency at 42.1%. The catalyst prepared at 450 °C exhibited the next highest efficiency, with a NO_x removal efficiency of 37.6%. In contrast, the catalyst calcined at 600 °C showed markedly reduced activity, with the performance not surpassing 20%.

Figure 3b presents the CH₄ conversion of the In/H-SSZ-39 catalysts. The conversion of CH₄ increased progressively with temperature, peaking at 500 °C. This suggested that a greater proportion of CH₄ participates in the activation reaction at this temperature, thereby enhancing the catalytic reduction of NO_x and the overall DeNO_x efficiency.

Figure 3c shows the CH₄ selectivity of the In/H-SSZ-39 catalysts across different calcination temperatures. The selectivity initially rose and then fell with increasing temperature, with the optimal selectivity at 500 °C. This trend was attributed to the increased likelihood of the methane combustion side reaction at higher temperatures, which reduces CH₄ selectivity. Notably, at 600 °C, CH₄ selectivity correlated positively with catalytic performance, with the highest selectivity observed for the catalyst calcined at 500 °C.

In our previous work [6], we established that the calcination temperature exerts a profound influence on the configuration of surface species. Specifically, the relative abundance of indium in diverse valence states was found to be a pivotal factor governing the catalytic proficiency of the respective catalysts. To further elucidate this phenomenon, we conducted XPS analyses on the In/H-SSZ-39 catalysts calcined at 450 °C, 500 °C, 550 °C, and 600 °C. The results of these analyses are presented in Figure 4 and Table 4.

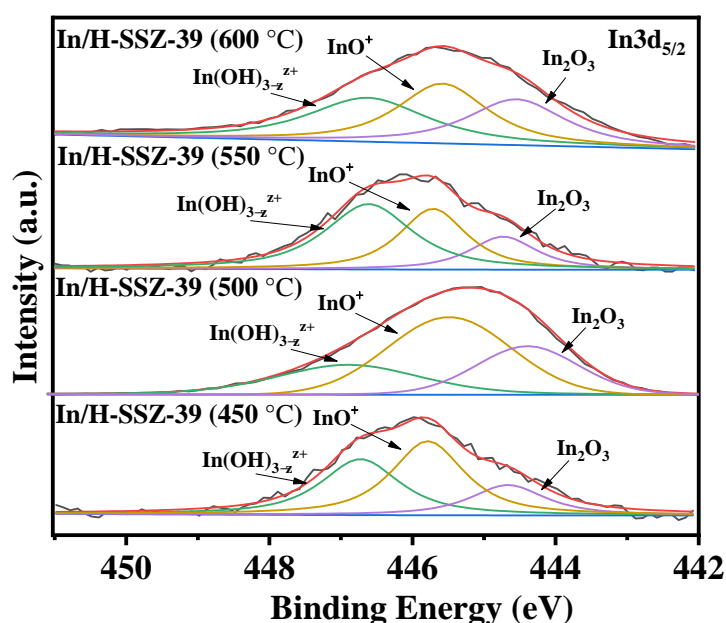


Figure 4. In 3d_{5/2} XPS spectra of the In/H-SSZ-39 prepared at different calcination temperatures.

Table 4. Surface element compositions in the In/H-SSZ-39 catalysts.

| Sample | InO ⁺ /(InO ⁺ + In ₂ O ₃ + In(OH) _{3-z} ^{z+}) |
|----------------------|--|
| In/H-SSZ-39 (450 °C) | 0.45 |
| In/H-SSZ-39 (500 °C) | 0.49 |
| In/H-SSZ-39 (550 °C) | 0.36 |
| In/H-SSZ-39 (600 °C) | 0.34 |
| Used In/H-SSZ-39 | 0.40 |

The high resolution In 3d_{5/2} spectra in Figure 4 could be deconvoluted into three indium chemical states, corresponding to In₂O₃ at ~445 eV, InO⁺ at ~446 eV, and In(OH)_{3-z}^{z+} species at ~447 eV [23–25]. Notably, InO⁺ was recognized as a crucial active site in the CH₄-SCR reaction, underscoring its significance in enhancing catalytic performance. An inspection of Table 4 revealed an intriguing trend in the ratio of InO⁺/(In₂O₃ + InO⁺ + In(OH)_{3-z}^{z+}), following the following sequence: In/H-SSZ-39 (600 °C) (0.34) < In/H-SSZ-39 (550 °C) (0.36) < In/H-SSZ-39 (450 °C) (0.45) < In/H-SSZ-39 (500 °C) (0.49). Notably, this ordering closely mirrors the observed CH₄-SCR activity of the respective catalysts.

Consequently, it was logical to deduce that the In/H-SSZ-39 catalyst exhibited superior catalytic activity when the ratio of $\text{InO}^+ / (\text{In}_2\text{O}_3 + \text{InO}^+ + \text{In}(\text{OH})_{3-z}^{z+})$ was maximized. This finding serves as conclusive evidence that the calcination temperature significantly influenced the ratio of surface-active species present in the catalyst, which in turn exerts a profound impact on its catalytic activity. Specifically, the variation in calcination temperature alters the distribution of indium in different valence states, notably In_2O_3 , InO^+ and $\text{In}(\text{OH})_{3-z}^{z+}$, with InO^+ being a pivotal active site in the CH_4 -SCR reaction. The observed correlation between the ratio of $\text{InO}^+ / (\text{In}_2\text{O}_3 + \text{InO}^+ + \text{In}(\text{OH})_{3-z}^{z+})$ and the catalytic activity underscores the critical role played by the surface composition in determining the overall performance of the catalyst. Therefore, by carefully controlling the calcination temperature, it is possible to optimize the ratio of these active species, thereby enhancing the catalytic activity of the In/H-SSZ-39 catalyst for CH_4 -SCR reactions.

2.1.3. Effect of In Ions Concentration

The loading of indium (In) on the catalysts was systematically varied by employing different concentrations of In ions in the ion-exchange solution. The In/H-SSZ-39 catalysts were synthesized using ion-exchange solutions with In concentrations of 0.033 M, 0.045 M, 0.066 M, and 0.08 M, each followed by a calcination step at 500 °C. The catalytic performance of the synthesized catalysts was evaluated under a NO concentration of 400 ppm, CH_4 concentration of 600 ppm, O_2 concentration of 10%, H_2O content of 6%, and GHSV of 21,000 h^{-1} .

Figure 5a illustrates the catalytic performance of the In/H-SSZ-39 catalysts as a function of the In ions concentration. The catalytic activity was observed to increase with increasing In concentration, reaching a peak, and then declining. Specifically, at an In concentration of 0.045 M, the In/H-SSZ-39 catalyst exhibited a maximum NO_x removal efficiency of 21.4%. This rate peaked at 42.1% for the catalyst prepared with a 0.066 M solution at 605 °C, beyond which the DeNO_x efficiency decreased to 35.1% at an In concentration of 0.08 M. Drawing from our prior research endeavors [6], it was observed that a continuous escalation in the In content occurred as the concentration of indium nitrate was augmented, which subsequently plateaued, signifying a diminishing rate of In content increase. Notably, the ICP analysis (Table 2) revealed that the catalytic activity peaked at an optimal In content of 5.2%, underscoring the crucial role of precise In incorporation in enhancing catalytic performance.

Figure 5b presents the CH_4 conversion of the In/H-SSZ-39 catalysts under various In ions concentration conditions. When the In ions concentration was 0.066 M, the In/H-SSZ-39 catalyst demonstrated superior CH_4 conversion at lower temperatures compared to other formulations, with minimal differences observed above 600 °C. At this temperature, CH_4 conversions were consistent across all catalysts at approximately 45%, except for the catalyst prepared with an 0.08 M solution, which showed a slightly lower conversion of 40%.

Figure 5c shows the CH_4 selectivity of the In/H-SSZ-39 catalysts. At a reaction temperature of 500 °C, when the In ions concentration was 0.066 M, the In/H-SSZ-39 catalyst displayed the highest CH_4 selectivity, followed by the 0.045 M In ions concentration. As the reaction temperature increased, the CH_4 selectivity of the catalysts decreased, likely due to the onset of the methane combustion side reactions.

In summary, the In/H-SSZ-39 catalyst prepared with an In ions concentration of 0.066 M and calcined at 500 °C exhibited the highest NO_x removal efficiency under hydrothermal conditions.

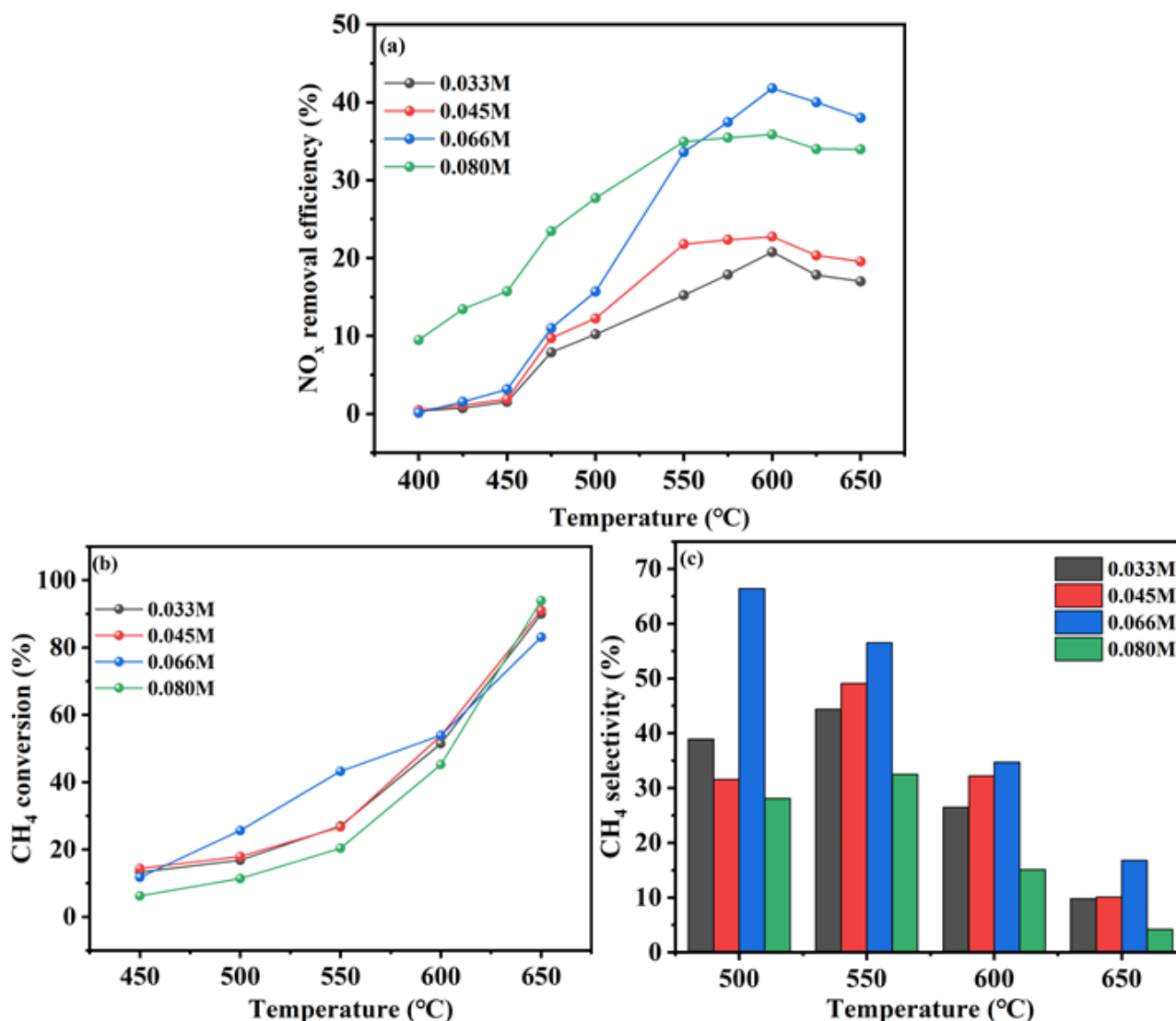
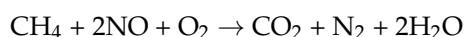


Figure 5. Catalytic performance of the In/H-SSZ-39 catalysts with various In ions concentrations. (a) NO_x removal efficiency, (b) CH₄ conversion, and (c) CH₄ selectivity.

2.2. Effect of Reaction Conditions

2.2.1. CH₄/NO Ratio

The CH₄-SCR process primarily removes NO_x through the reaction of methane, nitric oxide, and oxygen to form carbon dioxide, nitrogen, and water, which are non-polluting substances. The principal reaction is represented by the following equation [26]:



The ratio of methane to nitrogen is pivotal to the reaction's effectiveness and indicative of methane utilization efficiency across different CH₄/NO ratios. Experiments were conducted under the following conditions: a calcination temperature of 500 °C, an oxygen concentration of 10%, a steam concentration of 6%, a NO concentration of 400 ppm, and an airspeed of 21,000 h⁻¹, with argon as the equilibrium gas. The CH₄/NO ratio was varied by adjusting the methane concentration to ratios of 1, 1.5, and 2. The results are illustrated in Figure 6.

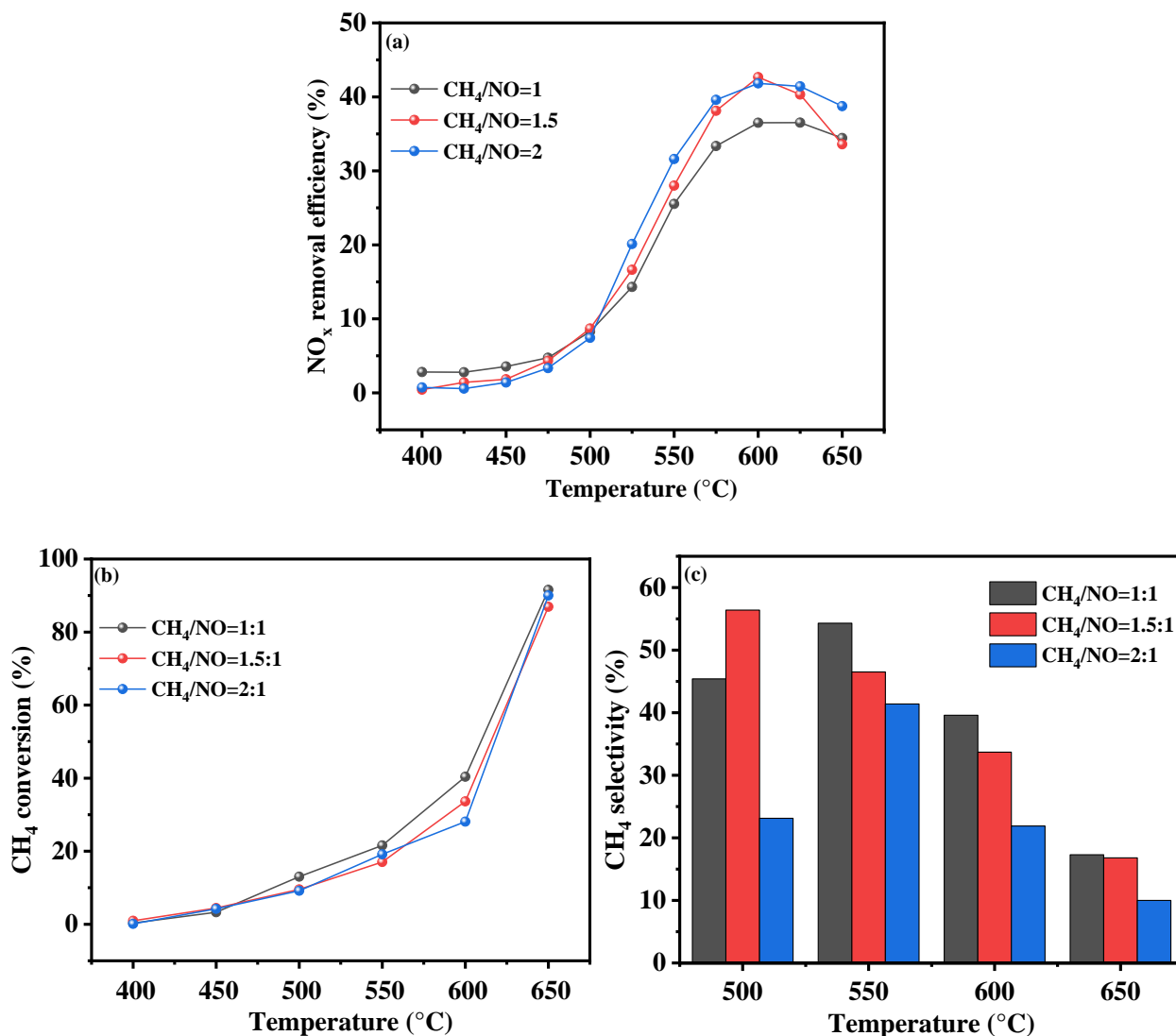


Figure 6. Catalytic performance of the In/H-SSZ-39 catalysts with various CH₄/NO ratios. (a) NO_x removal efficiency, (b) CH₄ conversion, and (c) CH₄ selectivity.

Figure 6a presents the NO_x removal efficiency of the In/H-SSZ-39 catalysts for various CH₄ to NO_x concentration ratios. The DeNO_x efficiency was observed to increase with the CH₄/NO ratio, particularly at temperatures above 500 °C. At CH₄/NO ratios of 1.5 and 2, the catalyst exhibited optimal performance at 600 °C, achieving the highest NO_x removal efficiency of 42.1%. At a CH₄/NO ratio of 1, the catalyst's NO_x removal efficiency peaked at 33.0%. From a cost-effectiveness perspective, a CH₄/NO ratio of 1.5 emerged as the most favorable reaction condition.

Figure 6b,c depicts the CH₄ conversion and selectivity of the In/H-SSZ-39 catalyst under hydrothermal conditions for different CH₄ to NO_x concentration ratios, respectively. Figure 6b indicates that the CH₄ conversion declined as the CH₄ to NO_x concentration ratio increased. A lower CH₄ to NO_x ratio resulted in a higher CH₄ conversion, with the In/H-SSZ-39 catalyst at a CH₄/NO ratio of 1.5 showing a 28.1% CH₄ conversion at 600 °C. Figure 6c demonstrates that CH₄ selectivity initially increased with temperature and then decreased. The highest CH₄ selectivity of 57.3% was recorded at a reaction temperature of 500 °C for a CH₄/NO_x ratio of 1.5. At 600 °C, CH₄ selectivity was positively correlated with catalytic performance, with the catalyst at a CH₄/NO ratio of 1.5 displaying a CH₄ selectivity of 35%. Consequently, subsequent experiments were conducted based on the 1.5/1 CH₄/NO ratio for further catalyst modification studies.

2.2.2. O₂ Concentration

Oxygen (O₂) plays a critical role as a reactant in the DeNO_x process. An insufficient concentration of O₂ may lead to incomplete reactions between methane and NO_x, while an excess can result in excessive combustion of methane. Therefore, determining the optimal O₂ concentration was crucial for maximizing the catalyst's performance. This section reports on the DeNO_x performance of the In/H-SSZ-39 catalyst at various O₂ concentrations, while keeping other experimental parameters constant. These parameters include the optimized preparation conditions (calcination temperature of 500 °C and an In concentration of 0.066 M) and reaction conditions (400 ppm NO, 600 ppm CH₄, 6% H₂O, and argon as the equilibrium gas). The oxygen concentrations tested were 5%, 8%, 10%, 15%, and 20%. The results are presented in Figure 7.

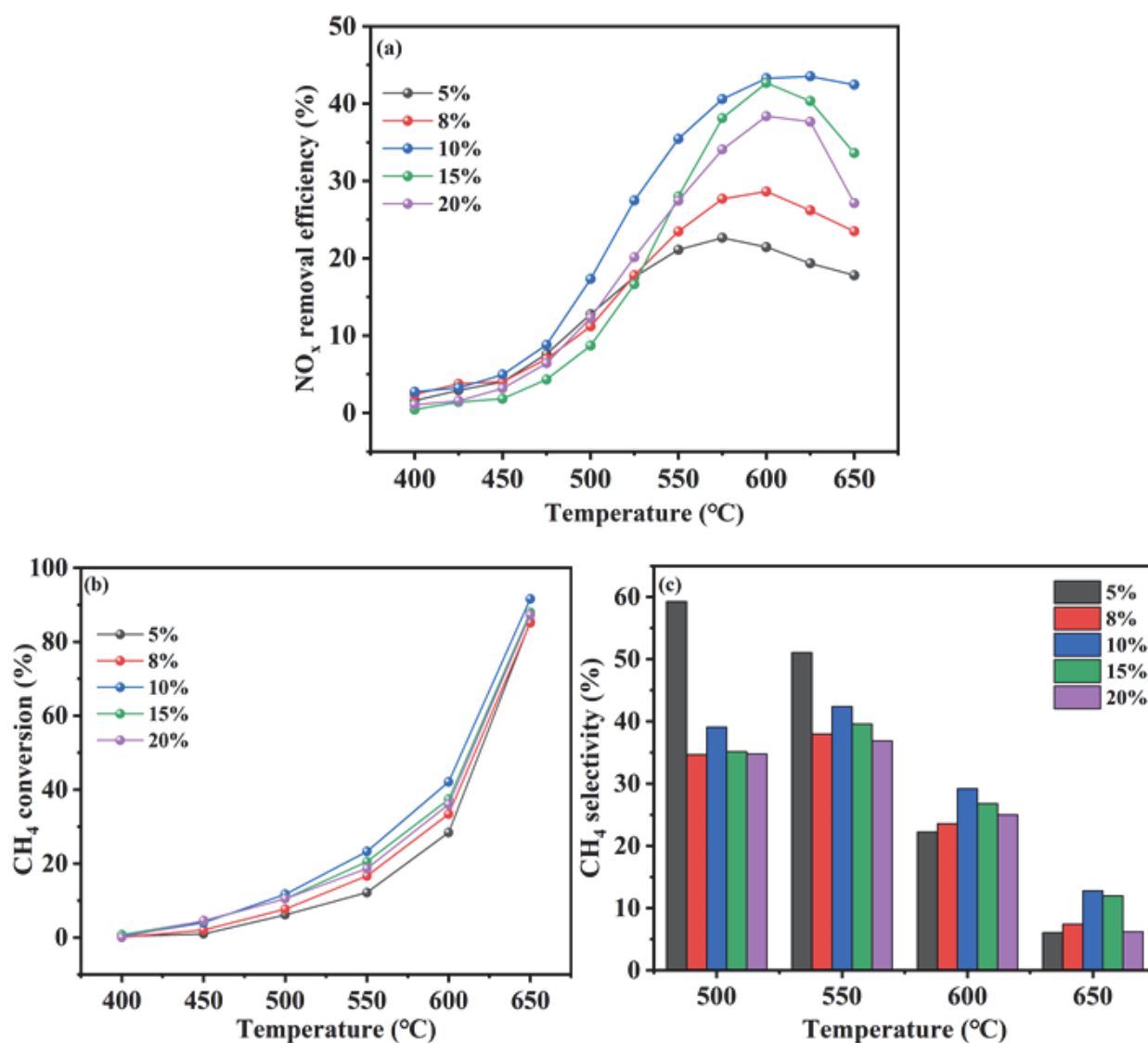


Figure 7. Catalytic performance of the In/H-SSZ-39 catalyst with various O₂ concentrations. (a) NO_x removal efficiency, (b) CH₄ conversion, and (c) CH₄ selectivity.

Figure 7a illustrates the NO_x removal efficiency of the In/H-SSZ-39 catalyst under hydrothermal conditions at different O₂ concentrations. The NO_x removal efficiency initially increases with O₂ concentration, reaching a peak, and then declines. Notably, the efficiency rose significantly from 5% to 10% O₂; under 5% O₂, the highest NO_x removal efficiency of 23.1% was achieved at 575 °C and under 10% O₂, 42.1% at 600 °C. At O₂

concentrations of 15% and 20%, the NO_x removal efficiency decreased, although the decline was less pronounced at 15%, indicating the catalyst's robustness against oxygen enrichment.

Figure 7b depicts the CH₄ conversion of the In/H-SSZ-39 catalyst under hydrothermal conditions at various O₂ concentrations. CH₄ conversion increased with temperature, with minimal differences observed between the concentrations tested. At 600 °C, the CH₄ conversion was 40.0% at 10% O₂ and approximately 33.0% at both 15% and 20% O₂. These results suggest that the In/H-SSZ-39 catalyst exhibited its best DeNO_x performance under an O₂ concentration of 10%.

Figure 7c shows the CH₄ selectivity of the catalyst under hydrothermal conditions across different O₂ concentrations. Between 400 °C and 550 °C, a lower O₂ concentration of 5% offered better CH₄ selectivity, possibly due to high O₂ concentrations promoting non-selective oxidation of CH₄. At 600 °C, CH₄ selectivity was comparable across all tested O₂ concentrations, with values of 30.5% at 10% O₂ and 27.4% at the 15% O₂ concentration.

In conclusion, subsequent experiments will be conducted based on the optimal reaction condition of an O₂ concentration of 10% for further catalyst modification studies.

2.2.3. Gaseous Hourly Space Velocity

Gaseous Hourly Space Velocity is a critical parameter in the industrial application of catalysts, as it affects the catalyst's ability to maintain high catalytic performance at high flow rates. In our experiment, the GHSV (Gas Hourly Space Velocity) of a catalyst is primarily calculated based on the volume of gas passing through a unit volume of catalyst per unit time. The formula for calculating GHSV is as follows:

$$\text{GHSV} = Q/V \quad (1)$$

where Q represents the total volumetric flow rate of the gas passing through the catalyst bed (This experiment is conducted at a flow rate of 100 mL/min). V is the volume of the catalyst bed or the catalyst volume used in the reaction (cm³).

In this experiment, the Gas Hourly Space Velocity (GHSV) is controlled by adjusting the catalyst volume, achieving values of 10,000 h⁻¹, 16,000 h⁻¹, 21,000 h⁻¹, and 30,000 h⁻¹.

This study investigates the impact of airspeed on the performance of In/H-SSZ-39 catalysts under hydrothermal conditions, with other experimental conditions held constant. These include a NO concentration of 400 ppm, a CH₄/NO ratio of 1.5, a H₂O concentration of 6%, and an O₂ concentration of 10%. The GHSVs tested were 10,000 h⁻¹, 16,000 h⁻¹, 21,000 h⁻¹, and 30,000 h⁻¹. The experimental results are depicted in Figure 8.

Figure 8a shows the CH₄-SCR NO_x removal efficiency of the In/H-SSZ-39 catalyst at various airspeeds and temperatures. The results indicated that lower GHSVs correspond to a higher NO_x removal efficiency, lower optimal activity temperatures, and broader activity windows. At an airspeed of 10,000 h⁻¹, the widest catalyst temperature window was observed, with the highest NO_x removal efficiency of 59.0% achieved at 590 °C. At an airspeed of 16,000 h⁻¹, the highest NO_x removal efficiency was 49.3% at 600 °C. The efficiencies were 41.9% and 39.5% at GHSVs of 21,000 h⁻¹ and 30,000 h⁻¹, respectively.

Figure 8b,c presents the CH₄ conversion and selectivity of the In/H-SSZ-39 catalyst at different GHSVs under hydrothermal conditions. Figure 8b demonstrates that CH₄ conversion generally increases with decreasing airspeed, approaching 100% at 650 °C for all airspeeds except 30,000 h⁻¹. Figure 8c revealed that while low GHSVs enhance NO_x removal efficiency and CH₄ conversion, they also reduced CH₄ selectivity, particularly in the temperature range of 500–600 °C. This suggested that at high temperatures, low airspeed did not improve CH₄ selectivity but instead promoted the selective oxidation of CH₄, thereby enhancing the DeNO_x activity of the catalyst.

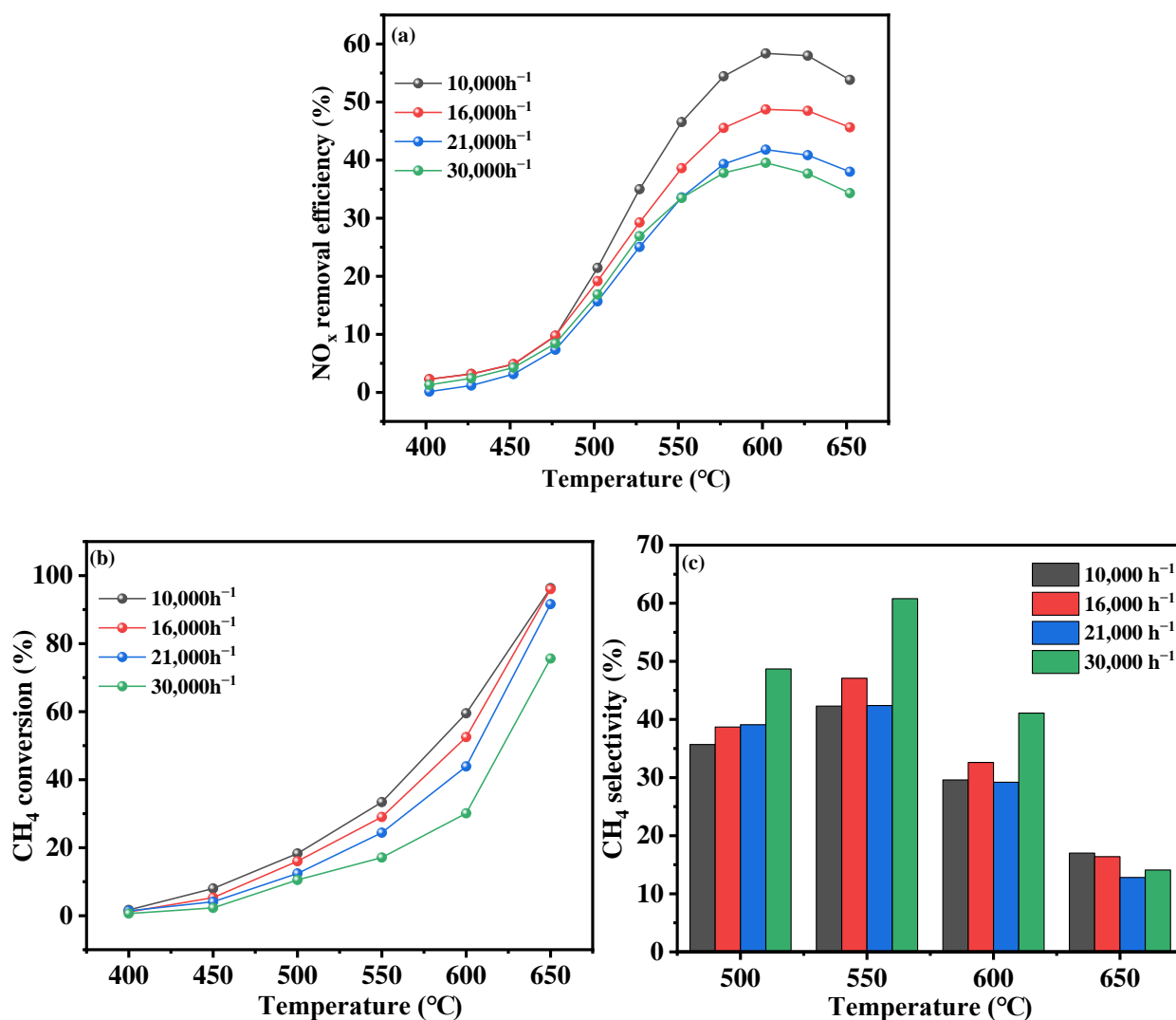


Figure 8. Catalytic performance of the In/H-SSZ-39 catalyst with various GHSVs. (a) NO_x removal efficiency, (b) CH₄ conversion, (c) CH₄ selectivity.

2.2.4. H₂O Concentrations

The ability of a catalyst to tolerate various concentrations of H₂O, particularly at high levels, is a crucial aspect of its performance, especially in industrial applications where hydrothermal conditions are common. This section presents experiments that assess the In/H-SSZ-39 catalyst's tolerance to H₂O while maintaining all other conditions constant: an O₂ of 10%, a CH₄/NO ratio of 1.5, and a NO_x concentration of 400 ppm. The H₂O concentrations tested were 0%, 5%, 10%, and 15%. The outcomes of these experiments are detailed in Figure 9.

Figure 9 illustrates the NO_x removal efficiency of the In/H-SSZ-39 catalyst under hydrothermal conditions at various steam levels. In the absence of H₂O, the catalyst demonstrates a broad activity temperature window, achieving over 70.0% NO_x removal at 550 °C. However, at a H₂O concentration of 5%, the efficiency at the same temperature drops to below 35.0%, indicating a significant impact of H₂O on the catalyst's DeNO_x performance. As H₂O concentration further increases, the negative effect intensifies, leading to a progressive decline in the DeNO_x performance. At a 10% H₂O concentration, the NO_x removal efficiency was reduced to only 19.2%.

Figure 9b depicts the CH₄ conversion of the In/H-SSZ-39 catalyst for the CH₄-SCR reaction across different water contents and reaction temperatures. The data indicated that methane conversion increases with temperature, with the highest rates occurring between 400–650 °C in the absence of H₂O, suggesting that water inhibited methane activation. At a reaction temperature of 600 °C, the methane conversion with 6% water content was 28.0%.

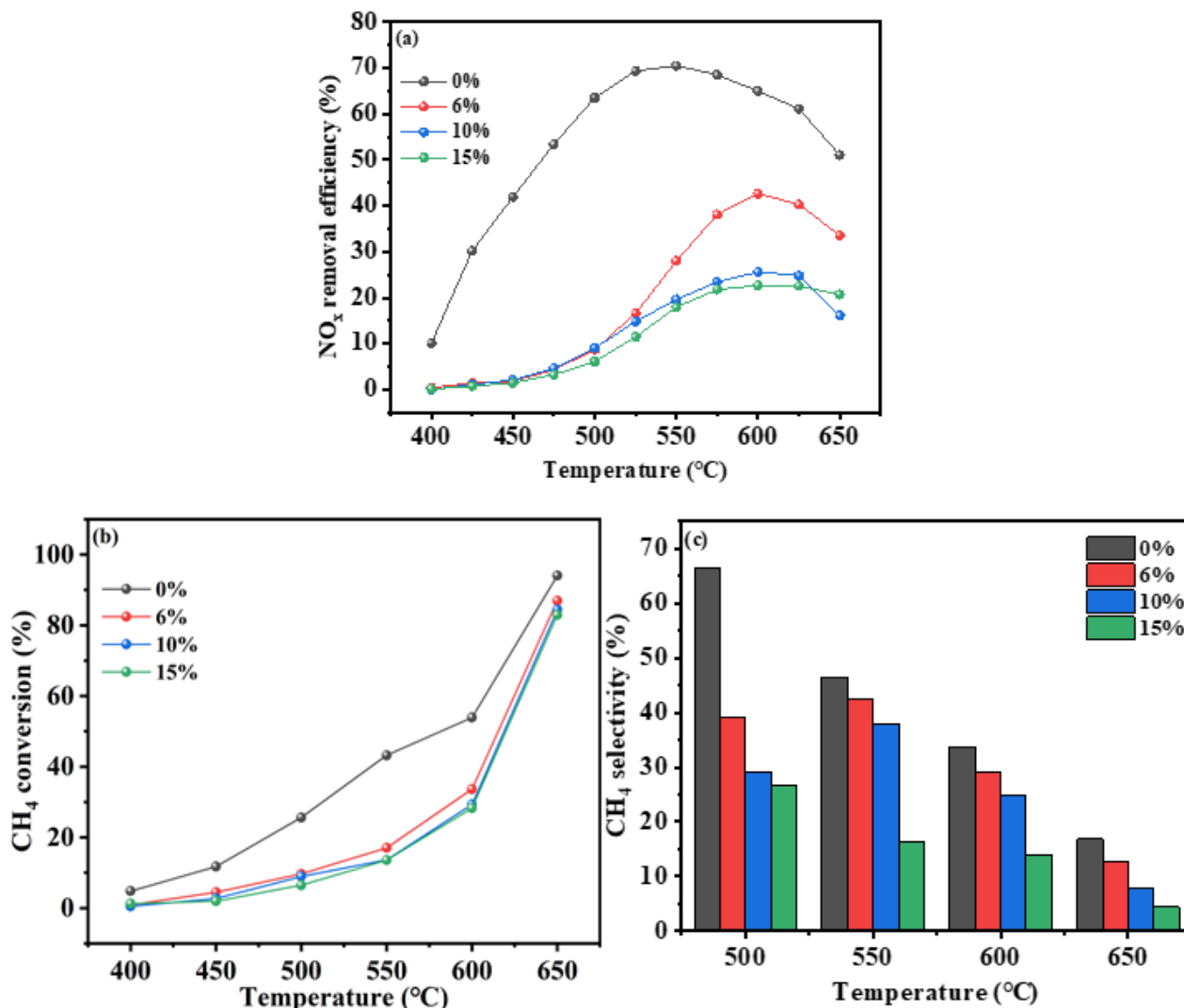


Figure 9. Catalytic performance of the In/H-SSZ-39 catalyst with various H₂O concentration. (a) NO_x removal efficiency, (b) CH₄ conversion, (c) CH₄ selectivity.

Figure 9c presents the CH₄ selectivity of the In/H-SSZ-39 catalyst at different water contents. Similar to conversion rates, CH₄ selectivity peaks when the reaction system was devoid of water, indicating that steam adversely affects both the conversion and selectivity of CH₄.

In summary, the experiments demonstrated that steam content significantly influenced the catalytic activity of the In/H-SSZ-39 catalyst. In corroboration with the literature [7,27,28], the catalyst's activity was also attenuated under conditions of high steam content, suggesting that water might occupy the active sites, thereby impeding the oxidation of NO and activation of CH₄, which consequently lead to a decrease in catalytic performance. Future work could focus on the enhancement of the SSZ-39 supported catalyst's activity through bimetallic modification to increase the number of active sites, presenting a potential avenue to improve the catalytic efficacy of the SSZ-39 zeolite under hydrothermal conditions.

2.3. Long Run Test

The preparation and reaction conditions were optimized as previously described, resulting in the specific conditions presented. Under these optimal conditions of 400 ppm NO, 600 ppm CH₄, 10% O₂, 10% H₂O, 21,000 h⁻¹, an extended operational duration was conducted. As depicted in the Figure 10, it is evident that the catalytic activity underwent a notable decline within the first 2 h, followed by a steady and slight downward trend. After 12 h of operation, the catalytic activity diminished by approximately 20%, indicating that the In/H-SSZ-39 catalyst possessed a certain degree of water resistance.

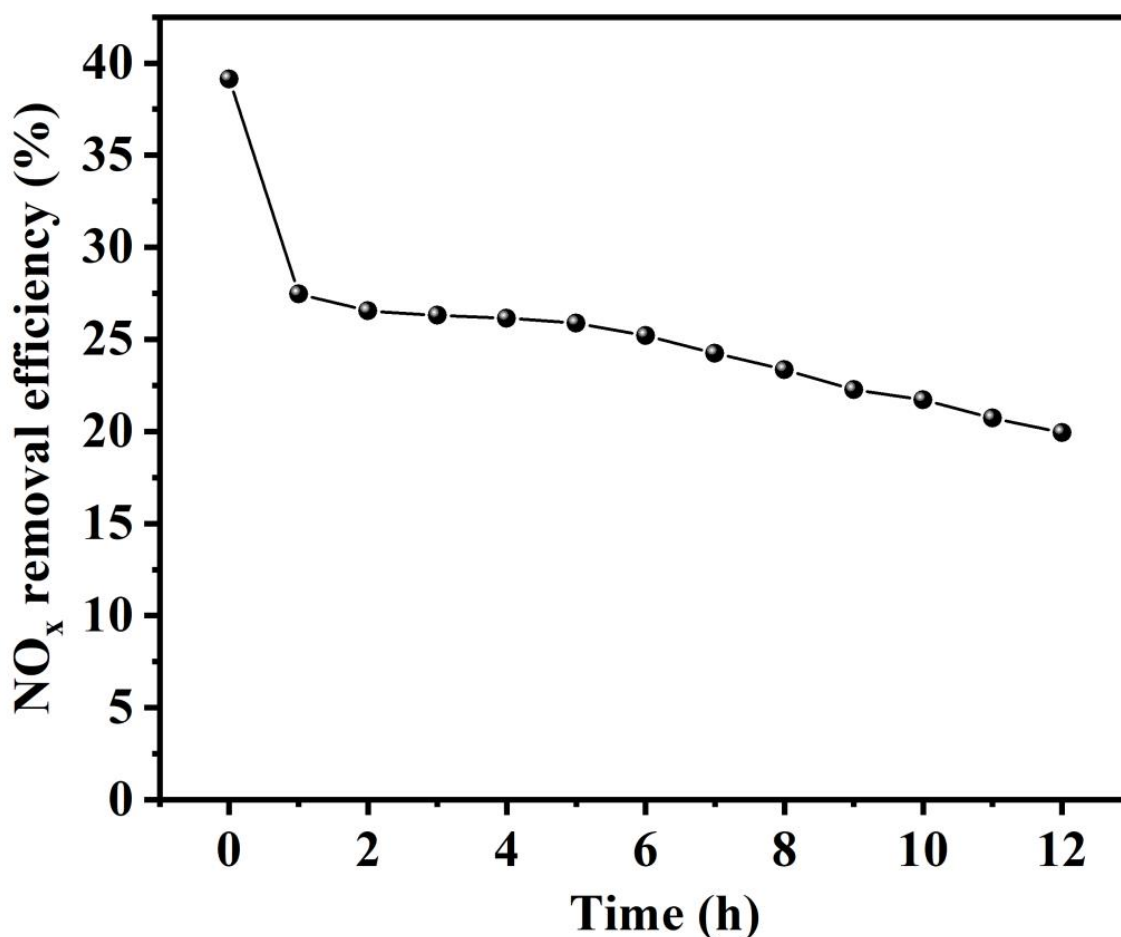


Figure 10. The long run test of the In/H-SSZ-39 catalyst.

2.4. Stability Test

To investigate the catalytic performance of the In/H-SSZ-39 catalyst during consecutive cyclic reactions under the presence of water, this section reports an experimental protocol where the conditions were maintained at 400 ppm NO, 600 ppm CH₄, 10% O₂, 6% H₂O, and a space velocity of 21,000 h⁻¹. The temperature was programmed to increase at a rate of 5 °C/min up to 650 °C, followed by a cooldown to room temperature. This temperature cycle was then repeated three consecutive times using the identical steps. The results of the three cyclic TPSR experiments are presented in Figure 11. As depicted in the Figure 11, during the consecutive second and third TPSR reactions, the NO_x removal efficiencies at 650 °C were 26.9% and 24.9%, respectively. This indicated that the In/H-SSZ-39 catalyst exhibited a certain degree of cyclic stability under aqueous conditions.

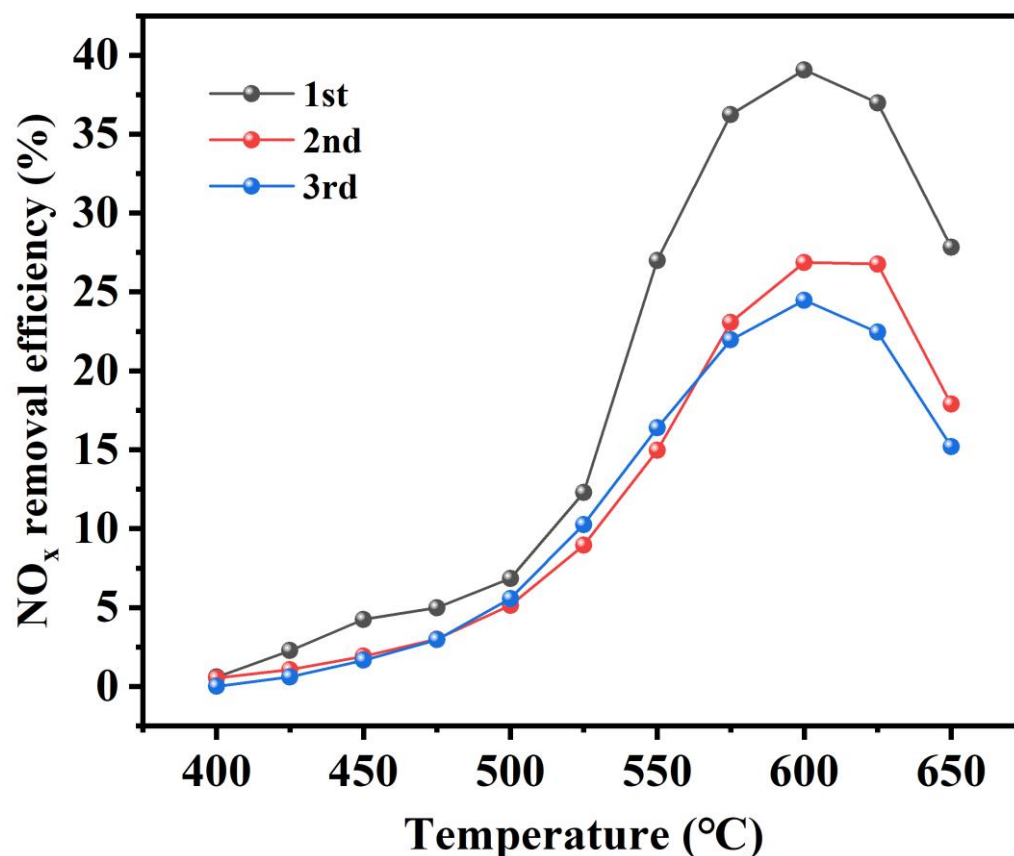


Figure 11. The stability test of the In/H-SSZ-39 catalyst.

2.5. Characteristics of Used In/H-SSZ-39 after CH₄-SCR in the Presence of H₂O

To gain a deeper understanding of the catalyst's performance, the evolution of key parameters including specific surface area, pore size distribution, phase composition, InO⁺ active species, and acidity, both prior to and subsequent to the reaction were studied.

The N₂ adsorption–desorption curves and pore size distribution plots of the catalyst, presented in Figure 12, reveal that the In/H-SSZ-39 catalyst exhibited a type IV N₂ adsorption–desorption isotherm, accompanied by an H4 hysteresis loop [29]. Notably, the pore size distribution plot (Figure 12) demonstrated a pronounced peak within the 2–5 nm range, indicative of a well-defined mesoporous structure. This mesoporous architecture was advantageous for facilitating the efficient diffusion of reactants and products during the catalytic DeNO_x reaction. The comprehensive analysis of pore properties is summarized in Table 5, indicating that prior to the reaction, the fresh In/H-SSZ-39 catalyst possessed a higher mesopore volume of 0.09 cm³g^{−1} compared to its post-reaction state. This observation suggested that during the reaction process, agglomeration of the active components or support particles might occur due to interparticle interactions, resulting in the formation of larger particles. Consequently, this agglomeration phenomenon led to a reduction in the interparticle voids, manifesting as a decrease in the mesopore volume.

Figure 13 presents the XRD spectra of the catalyst, analyzed prior to and subsequent to the reaction. Notably, both spectra exhibited characteristic peaks that are consistent with the SSZ-39 zeolite phase (PDF#45-0118) [17], indicating the structural integrity of the catalyst remained unaffected throughout the reaction process. Importantly, no discernible peaks associated with In₂O₃ were observed, which suggested that indium was successfully incorporated into the catalyst structure in the form of extra-framework cations, likely achieving a highly dispersed state. This finding underscores the successful incorporation and stabilization of indium within the SSZ-39 zeolite framework.

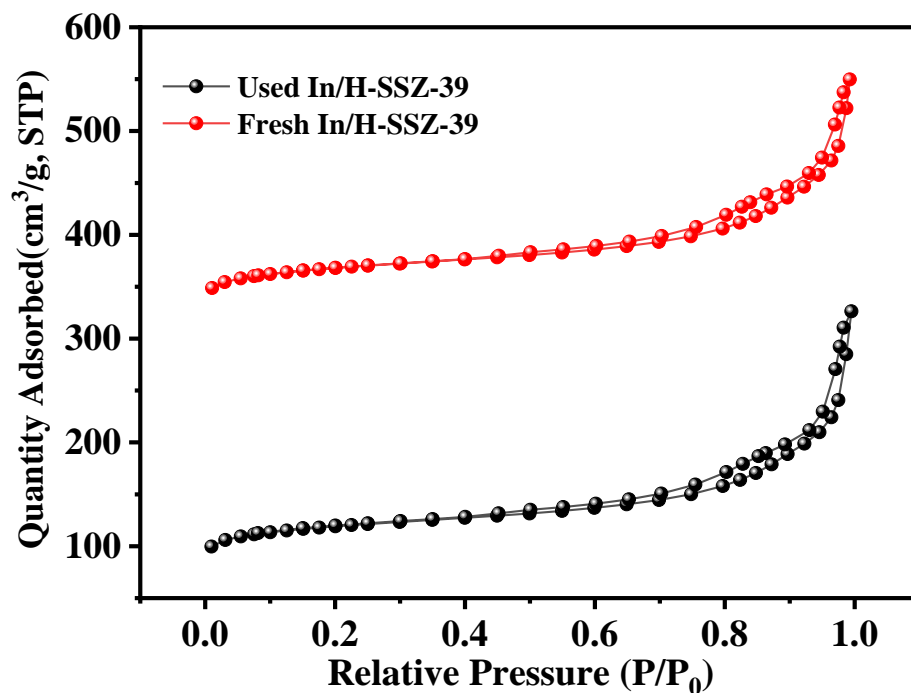


Figure 12. N_2 adsorption–desorption isotherms of the fresh and used In/H-SSZ-39 catalysts; the isotherms for the fresh and used In/H-SSZ-39 are vertically offset by $238 \text{ cm}^3/\text{g}$.

Table 5. Textural analysis of fresh and used In/H-SSZ-39 catalysts.

| Catalyst | S_{BET}^a (m^2g^{-1}) | V_{total}^b (cm^3g^{-1}) | V_{meso}^c (cm^3g^{-1}) | d_{meso}^d (nm) |
|-------------------|---|--|---|-----------------------------|
| Fresh In/H-SSZ-39 | 548.02 | 0.29 | 0.09 | 2.76 |
| Used In/H-SSZ-39 | 541.11 | 0.29 | 0.07 | 2.00 |

^a BET surface area obtained from the N_2 adsorption isotherm in the relative pressure range of 0.05–0.30. ^b Total pore volume calculated as the amount of N_2 adsorbed at $P/P_0 = 0.98$. ^c Mesopore volume calculated as total pore volume minus micropore volume obtained from a t-plot method. ^d Mesopore diameter calculated from the desorption branch using the BJH method.

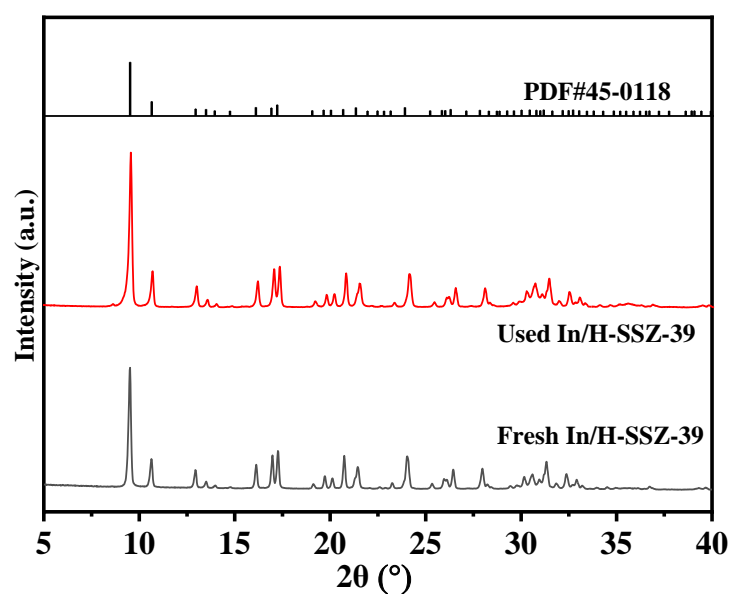


Figure 13. The XRD results of the fresh and used In/H-SSZ-39 catalysts.

Given the catalyst's declining stability under aqueous conditions, an exhaustive analysis of the post-reaction catalyst was conducted to further elucidate the mechanism. Figure 14 compares the XPS spectra of fresh and used In/H-SSZ-39 catalysts. Upon inspection, notable variations in the XPS spectra of the In/H-SSZ-39 catalyst were discernible before and subsequent to the reaction. According to the curve fitting in Table 4, for used In/H-SSZ-39 catalyst, the ratio of InO^+ / (InO^+ + In_2O_3 + $\text{In}(\text{OH})_{3-z}^{z+}$) was 0.40, which was lower than fresh In/H-SSZ-39 catalyst (0.49). The observed alterations in the active species prior to and subsequent to the reaction suggest that the experimental conditions have exerted a significant influence on the InO^+ species, resulting in a diminished capacity for NO oxidation and CH_4 activation. Consequently, this observation underscores the necessity for subsequent bimetallic modification of the SSZ-39 zeolites aimed at augmenting the catalyst's oxidation potential, ultimately enhancing its catalytic efficacy.

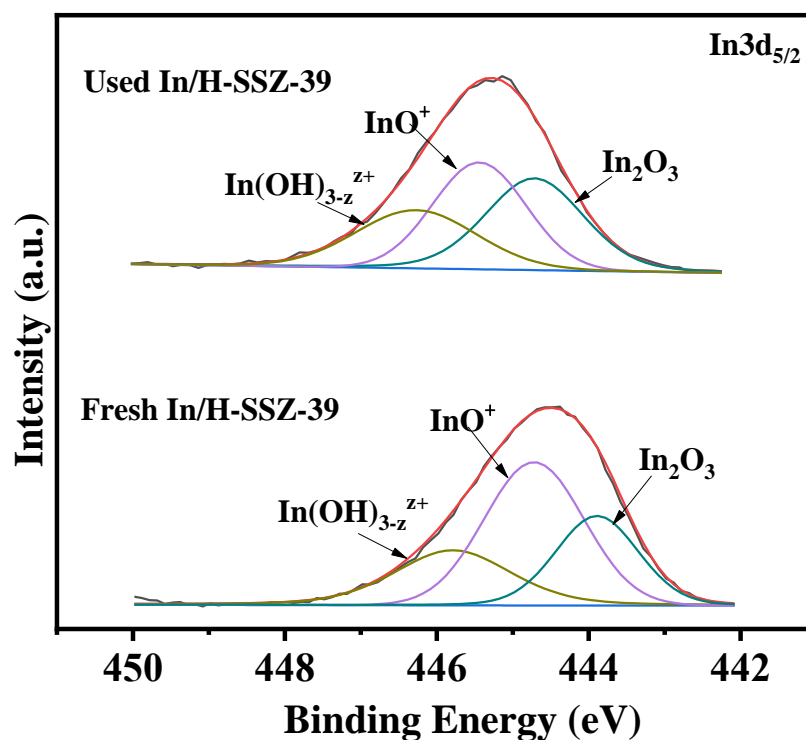


Figure 14. In $3d_{5/2}$ XPS spectra of the fresh and used In/H-SSZ-39 catalysts.

The NH_3 -TPD analysis of the In/H-SSZ-39 catalyst, conducted before and after undergoing the water-resistant CH_4 -SCR reaction, offered a profound insight into the alterations in surface acidities. As depicted in Figure 15 and Table 3, the experimental outcomes clearly revealed the changes. Notably, the employed In/H-SSZ-39 catalyst retained the presence of robust acid sites. It underscored a minimal perturbation in acidity during the CH_4 -SCR reaction process, hinting that the transformation of In_2O_3 into the pivotal InO^+ active species remains largely unimpeded [27].

In conclusion, during the CH_4 -SCR reaction process involving water, the crystal phase and acidity of the catalyst are not significantly affected. Nevertheless, the aggregation of surface-active components lead to a reduction in the mesopore volume. A decrease in the proportion of surface InO^+ species resulted in unsatisfactory catalyst stability and catalytic activity. In subsequent processes, the introduction of additional active components, such as bimetallic modification or metal oxide modification, will be necessary to enhance the oxidation performance of the catalyst, thereby improving its catalytic activity and stability.

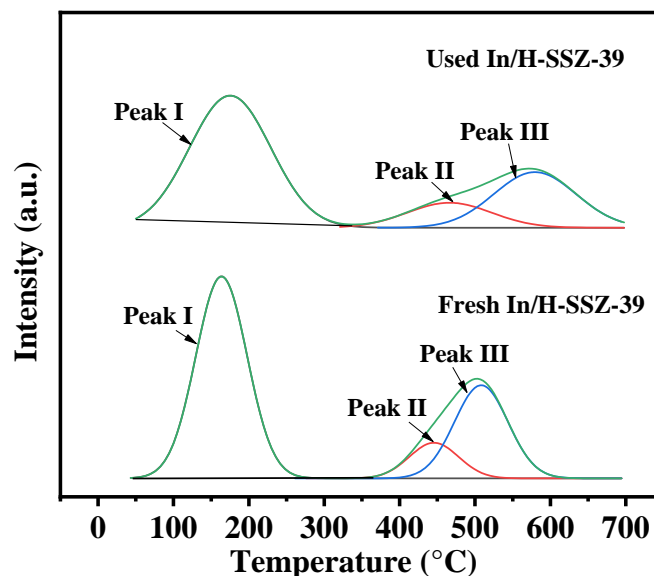


Figure 15. NH_3 -TPD plots of the fresh and used In/H-SSZ-39 catalysts.

3. Experimental

3.1. Catalyst Preparation

In this work, the liquid-phase ion-exchange method was used to synthesize the In/H-SSZ-39 catalysts using the following steps:

The synthesis began with the preparation of a 0.066 M $\text{In}(\text{NO}_3)_3 \cdot 4\text{H}_2\text{O}$ solution from 1 g of indium nitrate in 100 mL of deionized water. Subsequently, 3 g of H-SSZ-39 zeolites (Provided by the China Catalyst Holding Co., Ltd. from Dalian, China.) with a Si/Al ratio of 16 were introduced into the solution, which was then mixed thoroughly and magnetically stirred in a constant temperature water bath at 85 °C for 8 h. Post-stirring, the solution underwent centrifugal washing with deionized water five times. The resulting solid was dried in an oven at 80 °C for 12 h before being calcined in a muffle furnace at 500 °C under an air atmosphere for 3 h. The final catalyst was pressed, ground, and sieved through a 40–60 mesh sieve before being stored in a sample tube for subsequent activity evaluation.

In the optimization phase, variations were introduced to the synthesis process to fine-tune the catalyst's properties. For the optimization of indium content, different amounts of indium nitrate (1 g, 1.5 g, 2 g, and 2.5 g) were dissolved in 100 mL of deionized water during the initial step. Additionally, to determine the optimal calcination temperature, the catalysts were subjected to calcination at temperatures 450 °C, 500 °C, 550 °C, and 600 °C in the final step.

3.2. Catalytic Activity Measurements

Air path control system: The simulated flue gas used in the experiments was supplied from compressed standard gas cylinders. The primary gas composition consisted of NO/Ar (2000 ppm), CH_4 /Ar (5000 ppm), O_2 , SO_2 (100 ppm), and the carrier gas Ar. Steam was introduced using the bubbling method, where Ar gas was passed through a stainless-steel bubbler to carry it into the reaction gas stream. By combining the formula for the saturated vapor pressure of water, the water vapor content in the simulated flue gas could be controlled by adjusting the water temperature within the bubbler. Before entering the reaction gas stream, the gases from each cylinder were first regulated to a pressure of 0.1 MPa using secondary pressure reducing valves and pressure stabilizing valves. Subsequently, the flow rates of each gas stream were adjusted using mass flow controllers to achieve the desired gas concentrations. The individually prepared gas streams were then thoroughly mixed in a mixing tube before entering the reactor tube to participate in the thermocatalytic reaction.

Detection and analysis system: Upon traversing the catalytic reaction tube, the gas proceeds into the detection system, which encompasses the following: (1) A nitrogen oxides analyzer (Thermo Scientific-42i made in Thermo fisher scientific from Massachusetts, USA), adept at quantifying the concentrations of NO_x, NO, and NO₂ through the application of the chemiluminescence technique. (2) A gas chromatograph (GC 9790 II) is deployed for the determination of CH₄, CO, and CO₂ content, leveraging a flame ionization detector (FID) in conjunction with a Porapak-Q column. Throughout the detection process, nitrogen functions as the carrier gas, while hydrogen acts as the ignition gas, and dry air serves as the combustion-facilitating gas.

The activity evaluation experiments in this study [20,30] were conducted using programmed temperature-raising surface reaction (TPSR) experiments. The reaction gas components and their respective concentrations were specified as follows: NO (400 ppm), CH₄ (600 ppm), O₂ (10 %), and H₂O (6 %). Ar was utilized as a diluent gas to maintain a total flow rate of the mixed gases at 100 mL/min, with the GHSV controlled at 21,000 h⁻¹. The mixed reaction gas was passed into the quartz reaction tube at room temperature. Once NO_x reached adsorption equilibrium, the programmed temperature increase was initiated to perform the catalytic reaction. The temperature of the reactor was ramped up from 100–675 °C at a rate of 5 °C/min⁻¹. The contents of CH₄, CO, CO₂, NO_x, NO, NO₂, and N₂O were detected separately.

The catalytic activity of the catalyst for CH₄-SCR was assessed using the following parameters: NO_x removal efficiency (η), CH₄ conversion (γ), and CH₄ selectivity (α), calculated using Equations (2)–(4), respectively. Here, $c(\text{NO}_x)_{in}$ represents the initial concentration of NO_x, $c(\text{NO}_x)_{out}$ is the concentration of NO_x post-reaction, $c(\text{CH}_4)_{in}$ is the initial concentration of CH₄, $c(\text{CH}_4)_{out}$ is the concentration of CH₄ after the reaction, and $c(\text{N}_2)_{out}$ denotes the concentration of N₂ after the reaction.

$$\eta = \frac{c(\text{NO}_x)_{in} - c(\text{NO}_x)_{out}}{c(\text{NO}_x)_{in}} \times 100\% \quad (2)$$

$$\gamma = \frac{c(\text{CH}_4)_{in} - c(\text{CH}_4)_{out}}{c(\text{CH}_4)_{in}} \times 100\% \quad (3)$$

$$\alpha = \frac{0.5(c(\text{NO}_x)_{in} - c(\text{NO}_x)_{out})}{c(\text{CH}_4)_{in} - c(\text{CH}_4)_{out}} \times 100\% \quad (4)$$

3.3. Catalyst Characterizations

The indium, silicon, and aluminum content in the catalyst was determined by inductively coupled plasma atomic emission spectrometry (ICP-OES) analysis (Agilent, Technologies, Model 5100, California, USA). Crystallographic phases within the supports and catalysts were verified by X-ray Diffraction (XRD) analysis and recorded on a Rigaku D/MAX 2500PC diffractometer from Tokyo, Japan, utilizing a Cu K α radiation source operated at 40 kV and 200 mA, with a scanning rate of 4° per minute. The wide-angle 2 θ range scanned spanned from 5–40°, ensuring comprehensive phase identification. Nitrogen gas adsorption–desorption isotherms at –196 °C were obtained with a Micromeritics 2020 HD88 instrument (Georgia, USA), from which the Brunauer-Emmett-Teller (BET) surface areas (S_{BET}) were calculated. Mesopore size distribution was determined using the Barrett-Joyner-Halenda (BJH) model and micropore volumes were determined using a t-plot method. To gain insights into the electronic structure and chemical state of the catalyst surface, X-ray Photoelectron Spectroscopy (XPS) was conducted on an ESCALAB MK-II spectrometer (Glasgow, UK) from VG Scientific, utilizing an Al K α radiation source (1486.6 eV) for excitation. The acidity of the catalyst surface was determined by a temperature programmed desorption of ammonia (NH₃-TPD) experiment (MIC AutoChem1 II 2920 from Georgia, USA). Fifty milligrams of sample was loaded into a quartz reactor and pretreated in air at 500 °C for 1 h. After cooling to 50 °C, 10% NH₃/He was introduced at a flow rate of 50 mL/min for 1 h to saturate the sample with NH₃, followed by introducing

He flow as a purge gas. The NH₃-TPD profile was then recorded by a thermal conductivity detector (TCD) across the temperature range of 50–700 °C at a ramping rate of 10 °C/min.

4. Conclusions and Perspectives

In this paper, a novel In-H-SSZ-39 catalyst supported on a small-pore zeolite with an eight-membered ring framework was synthesized. The preparation conditions of the catalysts were optimized, and the effects of their reaction conditions were investigated. Moreover, a comprehensive suite of characterization techniques was employed to meticulously explore the mechanisms governing the influence of preparation conditions on catalytic activity, along with a meticulous investigation into the changes of physicochemical properties throughout the reaction process. The In/H-SSZ-39 catalyst exhibited a peak catalytic activity of 42.1% at 605 °C, under the optimized synthesis conditions where the indium ion concentration was 0.066 M and the calcination temperature was maintained at 500 °C. These findings were obtained under reaction conditions comprising a CH₄ concentration of 600 ppm, a NO concentration of 400 ppm, an O₂ concentration of 10 %, and a Gas Hourly Space Velocity (GHSV) of 21,000 h⁻¹. Furthermore, through a series of characterization analyses, it was observed that diverse preparation conditions exerted a profound influence on catalytic activity by modulating the quantity of acid sites and the proportion of surface-active species. In addition, the In/H-SSZ-39 catalyst exhibited promising catalytic activity within the realm of single-metal supported catalysts; yet there remains potential for further enhancement. During aqueous reactions, the crystalline phase and acidity of the catalyst undergo minimal alterations. However, a reduction in the proportion of surface InO⁺ species was noted, ultimately leading to suboptimal catalyst stability and catalytic activity. Future research endeavors could be directed towards augmenting the intrinsic activity of the SSZ-39 zeolite-supported catalyst by employing bimetallic or metallic oxide doping strategies, which might effectively amplify the availability of active sites. This approach holds promise as a viable strategy to bolster the catalytic potency of SSZ-39 under the demanding hydrothermal conditions prevalent in practical applications.

Author Contributions: Methodology, J.Z., J.J., M.W., J.C., J.L. and R.Z.; software, J.Z., J.J., M.W., J.C., J.L. and R.Z.; validation, J.Z.; formal analysis, J.Z., M.W., J.C. and J.L.; investigation, J.Z., J.J., M.W., X.W. and R.Z.; resources, J.Z., J.L., X.W. and R.Z.; data curation, M.W., J.C. and X.W.; writing—original draft preparation, J.Z. and M.W.; writing—review and editing, J.J. and R.Z.; project administration, R.Z.; funding acquisition, J.J. and R.Z. All authors have read and agreed to the published version of the manuscript.

Funding: We express our sincere gratitude for the financial support provided by the Special Project for Sustainable Development Science Technology in Shenzhen (KCXFZ20201221173000001), the Natural Science Foundation of Guangdong (No. 2022A1515011075), and the Special Foundation for Sustainable Development Research of Shenzhen (No. KCXST20221021111405012).

Data Availability Statement: Data will be made available on request.

Conflicts of Interest: Author Jin Li and Xianbin Wang were employed by the company China Catalyst Holding Co. The remaining authors declare that the research was conducted in the absence of any commercial or financial relationships that could be construed as a potential conflict of interest.

References

1. Lim, J.; Shin, J.; Ahn, N.; Heo, I.; Hong, S. Selective catalytic reduction of NO with CH₄ over cobalt-exchanged cage-based, small-pore zeolites with different framework structures. *Appl. Catal. B Environ. Energy* **2020**, *267*, 118710. [[CrossRef](#)]
2. Jing, G.; Li, J.; Yang, D.; Hao, J. Promotional mechanism of tungstated on selective catalytic reduction of NO_x by methane over In/WO₃/ZrO₂. *Appl. Catal. B Environ. Energy* **2009**, *91*, 123–134. [[CrossRef](#)]
3. Shan, Y.; Sun, Y.; Du, J.; Zhang, Y.; Shi, X.; Yu, Y.; Shan, W.; He, H. Hydrothermal aging alleviates the inhibition effects of NO₂ on Cu-SSZ-13 for NH₃-SCR. *Appl. Catal. B Environ. Energy* **2020**, *275*, 119105. [[CrossRef](#)]
4. Bellmann, A.; Atia, H.; Bentrup, U.; Brueckner, A. Mechanism of the selective reduction of NO_x by methane over Co-ZSM-5. *Appl. Catal. B Environ. Energy* **2018**, *230*, 184–193. [[CrossRef](#)]
5. Li, Y.; Armor, J. Selective catalytic reduction of NO with methane over metal exchanged zeolites. *Appl. Catal. B Environ. Energy* **1993**, *2*, 239–256. [[CrossRef](#)]

6. Zhao, J.; Zhang, G.; He, J.; Wen, Z.; Li, Z.; Gu, T.; Ding, R.; Zhu, Y.; Zhu, R. Effect of preparation and reaction conditions on the performance of In/H-Beta for selective catalytic reduction of NO_x with CH₄. *Chemosphere* **2020**, *252*, 126458. [[CrossRef](#)]
7. Zhao, J.; Chen, Y.; Wang, Y.; Li, Z.; Nkinahamira, F.; Zhu, R.; Li, C.; Zhang, J.; Sun, S.; Zhu, Y.; et al. The poisoning mechanism of H₂O/SO₂ to In/H-Beta for selective catalytic reduction of NO_x with methane. *Appl. Catal. A Gen.* **2023**, *649*, 118973. [[CrossRef](#)]
8. Kwak, J.; Tonkyn, R.; Kim, D.; Szanyi, J.; Peden, C. Excellent activity and selectivity of Cu-SSZ-13 in the selective catalytic reduction of NO_x with NH₃. *J. Catal.* **2010**, *275*, 187–190. [[CrossRef](#)]
9. Jo, D.; Ryu, T.; Park, G. Synthesis of high-silica LTA and UFI zeolites and NH₃-SCR performance of their copper-exchanged form. *ACS Catal.* **2016**, *6*, 2443–2447. [[CrossRef](#)]
10. Jo, D.; Park, G.; Ryu, T.; Hong, S. Economical synthesis of high-silica LTA zeolites: A step forward in developing a new commercial NH₃-SCR catalyst. *Appl. Catal. B Environ. Energy* **2019**, *243*, 212–219. [[CrossRef](#)]
11. Kim, J.; Cho, S.; Kim, D. Facile synthesis of KFI-type zeolite and its application to selective catalytic reduction of NO_x with NH₃. *ACS Catal.* **2017**, *7*, 6070–6081. [[CrossRef](#)]
12. Ming, S.; Chen, Z.; Fan, C. The effect of copper loading and silicon content on catalytic activity and hydrothermal stability of Cu-SAPO-18 catalyst for NH₃-SCR. *Appl. Catal. A Gen.* **2018**, *559*, 47–56. [[CrossRef](#)]
13. Chen, Z.; Fan, C.; Pang, L.; Ming, M.S.; Guo, W.; Liu, P.; Chen, H.; Li, T. One-pot synthesis of high-performance Cu-SAPO-18 catalyst for NO reduction by NH₃-SCR: Influence of silicon content on the catalytic properties of Cu-SAPO-18. *Chem. Eng. J.* **2018**, *348*, 608–617. [[CrossRef](#)]
14. Corma, A.; Puche, M.; Rey, F.; Sankar, G.; Teat, S.J. A zeolite structure (ITQ-13) with three sets of medium-pore crossing channels formed by 9- and 10-Rings. *Angew. Chem. Int. Ed.* **2003**, *42*, 1156–1159. [[CrossRef](#)] [[PubMed](#)]
15. Kwak, J.H.; Tran, D.; Burton, S.D.; Szanyi, J.; Lee, J.H.; Peden, C.H.F. Effects of hydrothermal aging on NH₃-SCR reaction over Cu/zeolites. *J. Catal.* **2012**, *287*, 203–209. [[CrossRef](#)]
16. Fickel, D.W.; D'Addio, E.; Lauterbach, J.A. The ammonia selective catalytic reduction activity of copper-exchanged small-pore zeolites. *Appl. Catal. B Environ. Energy* **2011**, *102*, 441–448. [[CrossRef](#)]
17. Du, J.; Han, S.; Huang, C.; Shan, Y.; Zhang, Y.; Shan, W.; He, H. Comparison of precursors for the synthesis of Cu-SSZ-39 zeolite catalysts for NH₃-SCR reaction. *Appl. Catal. B Environ. Energy* **2023**, *338*, 123072. [[CrossRef](#)]
18. Zhao, J.; Wen, Z.; Zhu, R.; Li, Z.; Ding, R.; Zhu, Y.; Gu, T.; Yang, R.; Zhu, Z. In/H-Beta modified by Co₃O₄ and its superior performance in the presence of H₂O and SO₂ for selective catalytic reduction of NO_x with CH₄. *Chem. Eng. J. Adv.* **2020**, *3*, 100029. [[CrossRef](#)]
19. Chen, S.; Yan, X.; Wang, Y.; Chen, J.; Pan, D.; Ma, J.; Li, R. Effect of SO₂ on Co sites for NO-SCR by CH₄ over Co-Beta. *Catal. Today* **2011**, *175*, 12–17. [[CrossRef](#)]
20. Zhao, J.; Dong, L.; Wang, Y.; Zhang, J.; Zhu, R.; Li, C.; Hong, M. Amino-acid modulated hierarchical In/H-Beta zeolites for selective catalytic reduction of NO with CH₄ in the presence of H₂O and SO₂. *Nanoscale* **2022**, *14*, 5915–5928. [[CrossRef](#)]
21. Yang, J.; Chang, Y.; Dai, W.; Wu, G.; Guan, N.; Li, L. Ru-In/H-SSZ-13 for the selective reduction of nitric oxide by methane: Insights from temperature-programmed desorption studies. *Appl. Catal. B Environ. Energy* **2018**, *236*, 404–412. [[CrossRef](#)]
22. Gruttadauria, M.; Giacalone, F.; Noto, R. Supported proline and proline-derivatives as recyclable organocatalysts. *Chem. Soc. Rev.* **2008**, *37*, 1666–1688. [[CrossRef](#)] [[PubMed](#)]
23. Zamaro, J.; Miró, E.; Boix, A.; Hernandez, A.; Fuentes, G. In-zeolites prepared by oxidative solid state ion exchange (OSSIE): Surface species and structural characterization. *Micropor. Mesopor. Mat.* **2010**, *129*, 74–81. [[CrossRef](#)]
24. Lónyi, F.; Solt, H.E.; Valyon, J.; Boix, A.; Gutierrez, L.B. The activation of NO and CH₄ for NO-SCR reaction over In- and Co-containing H-ZSM-5 catalysts. *J. Mol. Catal. A Chem.* **2011**, *345*, 75–80. [[CrossRef](#)]
25. Ogura, M.; Ohsaki, T.; Kikuchi, E. The effect of zeolite structures on the creation of InO⁺ active sites for NO_x reduction with methane. *Micropor. Mesopor. Mat.* **1998**, *21*, 533–540. [[CrossRef](#)]
26. Khan, A.; Kennedy, M.; Dlugogorski, B.Z. Partial oxidation of methane with nitrous oxide forms synthesis gas over cobalt exchanged ZSM-5. *Catal. Commun.* **2014**, *53*, 42–46. [[CrossRef](#)]
27. Zhao, J.; Li, Z.; Zhu, R.; Zhang, J.; Ding, R.; Wen, Z.; Zhu, Y.; Zhang, G.; Chen, B. Mechanism of the selective catalytic reduction of NO_x with CH₄ on In/H-beta. *Catal. Sci. Technol.* **2021**, *11*, 5050–5061. [[CrossRef](#)]
28. Shi, Y.; Pu, J.; Gao, L.; Shan, S. Selective catalytic reduction of NO with NH₃ and CH₄ over zeolite supported indium-cerium bimetallic catalysts for lean-burn natural gas engines. *Chem. Eng. J.* **2021**, *403*, 126394. [[CrossRef](#)]
29. Thommes, M.; Kaneko, K.; Neimark, A.V.; Olivier, J.P.; Rodriguez-Reinoso, F.; Rouquerol, J.; Sing, K.S.W. Physisorption of gases, with special reference to the evaluation of surface area and pore size distribution (IUPAC Technical Report). *Pure Appl. Chem.* **2015**, *87*, 1051–1069. [[CrossRef](#)]
30. Zhao, J.; Li, H.; Wang, Y.; Zhu, R.; Sun, S.; Zhang, J.; Li, C.; Hong, M. Desilication tuning of In/Hβ catalysts for sulfur- and steam-resistant CH₄-SCR of NO. *Catal. Commun.* **2023**, *175*, 106619. [[CrossRef](#)]

Disclaimer/Publisher's Note: The statements, opinions and data contained in all publications are solely those of the individual author(s) and contributor(s) and not of MDPI and/or the editor(s). MDPI and/or the editor(s) disclaim responsibility for any injury to people or property resulting from any ideas, methods, instructions or products referred to in the content.